Revealing the microstructural stability of a three-phase soft solid (ice cream) by 4D synchrotron X-ray tomography

Enyu Guo [a,b,**], Daniil Kazantsev [a,b], Jingyi Mo [a,b], Julian Bent [c], Gerard Van Dalen [c], Peter Schuetz [c], Peter Rockett [a], David StJohn [d], Peter D Lee [a,b,*]

[a] School of Materials, The University of Manchester, Manchester, M13 9PL, U. K

[b] Research Complex at Harwell, RAL, Didcot, OX11 0FA, U. K

[c] Unilever R&D, Colworth, MK44 1LQ, U. K

[d] School of Mechanical and Mining Engineering, The University of Queensland, St Lucia, Queensland, 4072, Australia

Submitted to

Journal of Food Engineering

January 2018

[*, **]Corresponding authors:
[*]Peter D Lee: peter.lee@manchester.ac.uk; Tel: +44 (0)1235 567789
[**]Enyu Guo: enyu.guo@manchester.ac.uk; Tel: +44 (0)1235 567886

Abstract

Understanding the microstructural stability of soft solids is key to optimizing formulations and processing parameters to improve the materials' properties. In this study, *in situ* synchrotron X-ray tomography is used to determine the temperature dependence of ice-cream's microstructural evolution, together with the underlying physical mechanisms that control microstructural stability. A new tomographic data processing method was developed, enabling the features to be segmented and quantified. The time-resolved results revealed that the melting-recrystallization mechanism is responsible for the evolution of ice crystal size and morphology during thermal cycling between -15 and -5 ^{o}C, while coalescence of air cells is the dominant coarsening mechanism controlling air bubble size and interconnectivity. This work also revealed other interesting phenomena, including the role of the unfrozen matrix in maintaining the ice cream's microstructural stability and the complex interactions between ice crystals and air structures, e.g. the melting and recrystallization of ice crystals significantly affect the air cell's morphology and the behavior of the unfrozen matrix. The results provide crucial information enhancing our understanding of microstructural evolution in multi-phase multi-state complex foodstuffs and other soft solids.

Keywords: Ice cream; Microstructure; Tomography; Ice crystals; Coarsening; Soft solid.

1. Introduction

Soft solids are important composites that are characterized by complex multi-phase structures and possess inherently complex non-Newtonian rheological properties under external stress [1-3]. Soft solids exist either in nature, e.g. muds, or in many artificially manufactured products such as emulsions, biopolymers, fresh concrete and domestic baking materials. Many soft solids, such as soft foams (e.g. ice cream) and aerated desserts, contain porous phases within a viscous matrix [4-6].

Structural stability is desired for many soft foams and microstructural instability greatly influences the materials' properties and their applications. Take ice cream for example. The microstructure of ice cream, including the size distribution and connectivity of each phase, plays a critical role in determining product quality (e.g. mouthfeel, taste, appearance, etc.) and the product's shelf-life [6-10]. For example, the microstructural change at different storage temperatures has been shown to alter ice cream's viscoelastic properties and and hence our oral sensory perception of it [10]. However, irreversible microstructural changes often occur in ice creams (over a range of different timescales), as well as in other similar foam structures that contain air, above a certain temperature (~ -30 °C for ice cream [4]) which may occur during shipping, storage at the grocery store and in domestic freezers (ca. -18 ºC), and on the consumer's table.

For ice cream, the structural instability is affected by many factors, including compositions [11, 12] and thermal variations [5, 13]. One of the well-recognized phenomena due to thermal instability is coarsening of microstructure [4, 5, 13-15]. This was initially examined in light microscopy [14, 16-19] and cryo-scanning electron

microscopy [20, 21], and transmission electron microscopy [22], all of which provide only 2D information of the surface or of cuts through the ice cream sample. These phenomena were recently studied in 3D with X-ray tomography on *ex situ* coarsened samples [4, 5]. Using a synchrotron X-ray tomography technique, we revealed in our previous work [5] that after thermal cycling (or thermal 'abuse') between -15 and -5 ^{o}C for a number of cycles/days, both ice crystals and air cells grew in size creating ice dominated structures within a deteriorated ice cream microstructure. More specifically, the size of ice crystals was observed to continuously increase up to 14 cycles; however, the growth rate significantly decreased after 7 thermal cycles. The air cells also increased in size, and they continued to grow into interconnected irregular shapes with long continuous channels after 14 thermal cycles. However, for up to 7 thermal cycles the air cells seemed to remain more or less spherical.

From that *ex situ* study, we also observed that the ice crystals within the unfrozen matrix tended to align along the boundary between air cells and the matrix, minimizing surface energy. Our findings in those 3D experiments provided valuable insight into the structural changes of ice cream upon thermal cycling. However, the study was performed on *ex situ* thermally cycled samples and thus, the interactions between the microstructural features could not be elucidated. The detailed mechanisms that control the microstructural evolution, which are only available via *in situ* studies, still remain to be explored. Questions regarding the growth mechanisms and relative movement of the phases and their exact interactions during thermal cycling, need to be answered to be able to improve the stability of the ice cream's structure [5, 14, 23]. For example,

what are the dynamics of the changes for each phase and how do they impose on each other due to thermal variations, in order to maintain the integrity of ice cream's structure? What are the dominant coarsening mechanisms that control the ice cream's microstructural evolution?

This work non-destructively studies the thermal stability of the ice cream microstructure via 4D (3D plus time) synchrotron X-ray tomography to reveal the dynamics of the microstructural changes. This technique has become increasingly used in the study of opaque materials systems to study both coarsening [24] and rheology during deformation [25, 26]. X-ray tomographs were continuously acquired on a sample during a heating and cooling cycle at a well-controlled slow ramp rate of 0.05 ^{o}C/min. To analyze the acquired data, an iterative tomographic data reconstruction and image processing method was developed. Through quantitative analysis, the physical mechanisms which dominate the degradation of ice cream's microstructure due to temperature variation, are examined and discussed in detail.

2. Materials and methods

2.1 Sample and experimental methods

Fresh ice cream containing 5% fat was manufactured by Unilever R&D (U. K). A 500 ml block of fresh ice cream was initially thermally cycled between -15 and -5 ^{o}C for seven times (1 week) before it was used for the *in situ* synchrotron experiment. The seven cycles created a larger scale of microstructure, enabling easy identification of phases for quantification, and also represent a transition point between the observations made in the first seven cycles where change was relatively rapid and the next seven

cycles where the size of ice crystals became more stable as reported in our *ex situ* studies [5]. Small ice cream samples, each contained in a 3 mm inner diameter kapton tube (67 μm thick, American Durafilm Co. Inc, Holliston, U.S), were cut from the 500 ml block. Details of the sample preparation method are described in [5].

The *in situ* synchrotron experiment was conducted on the Diamond Manchester Beamline (I13-2) of the Diamond Light Source (DLS, U.K) using a pink beam. The set-up for running the beamline experiment, together with the cold stage used to provide the sample temperature, is described in [5, 27]. During the *in situ* thermal cycling experiment, the sample was loaded in the cold stage at -15 ^{o}C and stabilized for 10 min. Then, the sample was heated to -5 ^{o}C at a ramp rate of 0.05 K/min and held there for 10 min. After that, the sample was cooled back to -15 ^{o}C at the same ramp rate as the heating stage. A schematic of the thermal cycle history is shown in the inset of Fig. 1. The tomographic scans were acquired using a 2560 × 2160 pixel PCO Edge 5.5 CMOS camera that was optically coupled to a single crystal $CdWO_4$ scintillator during the thermal cycle. For each tomographic scan, 900 projections were recorded with an exposure time of 100 ms (90 s for each scan) and a pixel size of 0.8 μm. However, at the end of each tomographic scan, the sample stage was rotated back to the initial position for system re-initiation to start the next tomographic scan, adding an additional delay of ~ 51s, for a cycle time of ~ 141 s. In total, 178 tomographic scans were acquired during a thermal cycle.

2.2 Image reconstruction and three-phase segmentation approach

Initially, the acquired projection data were reconstructed using the conventional

Filtered Back Projection (FBP) algorithm [28], producing extremely noisy reconstructions with low contrast and ring artifacts (see Fig. 2(a)). The poor quality of FBP images was due to angular under-sampling (only 900 projections for a 2k × 2k × 2k volume), short exposure time and low attenuation contrast between ice and water. In order to improve the image quality suitable for segmentation, we applied a Model-Based Iterative Reconstruction (MBIR) approach.

Our MBIR algorithm is based on the Group-Huber data fidelity function to minimize ring artifacts and 3D total variation (TV) regularization penalty [29-31]. . The TV-related regularization sub-problem has been solved using the Split-Bregman method in order to enhance the weak contrast between ice crystals and unfrozen matrix (see Fig. 2(b)).

Although MBIR reconstruction substantially improves the contrast and also removes noise, the reconstructed images suffer from the visible intensity inhomogeneities within various ice-crystals (indicated by arrows in Fig. 2(b)). These artifacts can be a result of the combined effects of strong noise and beam hardening. The latter is possible due to abrupt changes in attenuation coefficients between unfrozen matrix (highly attenuated) and ice crystals (poorly attenuated), therefore introducing non-linearity in a beam. Intensity inhomogeneity within a single crystal restricts successful segmentation by histogram thresholding. One can use more sophisticated segmentation methods (e.g. 3D snake contours can successfully segment features with intensity inhomogeneity using supervised seeding). However, due to the large data size, a computationally efficient approach is required.

Here we applied an additional post-processing step to equalize intensity within phases by means of gradient-constrained nonlinear isotropic diffusion [5, 32]. The mask to terminate the diffusion process across selected boundaries was acquired from the image in Fig. 2(b) by thresholding the magnitude of the gradient. Since the gradient magnitude between phases is large and the variations of intensity within regions are gradual, one can run the constrained diffusion until the regions become fully homogeneous. Therefore, we run 1000 diffusion iterations on GPU to equalize intensities within enclosed regions of the image in Fig. 2(b). The result (Fig. 2(c)) is sufficient to implement a simple histogram thresholding operation and generate images with homogeneous contrast within three phases (Fig. 2(d)).

Finally, the processed volume was cropped into a smaller volume for 3D analysis. 3D rendering of the features, as well as quantification of size/volume, was performed using Avizo® (FEI, Thermo Fisher Scientific, U. S). The thickness of unfrozen matrix was measured using BoneJ in ImageJ [33].

3. Results and Discussion

3.1 General microstructural evolution during thermal cycling

Fig. 3 and supplementary video 1 show the 2D tomographic slices of ice cream's microstructural evolution during thermal cycling between -15 and -5 ^{o}C. A few salient observations can be made based on these images. First, ice crystals were continuously melting, decreasing in size, during the heating stage (Fig. 3(a-c)) and their morphologies became more spherical at "high" temperature (e.g. -5 ^{o}C, Fig. 3(c)). It

appears that the most significant morphologic change took place in the temperature range -7.5 to -5 ^{o}C. During cooling, the relatively round ice crystals grow into a more irregular morphology again (Fig. 3(d-f)), as expected for ice which has a high anisotropy in interfacial energy. Second, some of the air cells tended to coalesce. One example is indicated by the arrows in Fig. 3(a) and (b), where two neighboring large air cells gradually merged into one.

Third, it is observed that during the heating stage the microstructural features moved to the upper right corner of the region in Fig. 3, and observed more clearly in supplementary video 1, because of the volume shrinkage when ice crystals were melted into the unfrozen matrix. An air cell in Fig. 3(b) (indicated by a red arrow) shows the example of this movement. Note that the microstructure seemed to be compressed slightly due to the decreasing volume. It is mentioned that the expansion of volume seemed to be less significant during cooling as compared to the reduction in volume upon heating. The degree of expansion and relative movement during cooling also suggests the unfrozen matrix is quite flexible in response to external thermal change at high temperatures.

Microstructures in the longitudinal section were extracted for further examination and the results are shown in supplementary Fig. S1. The microstructural features (e.g. ice crystals and air cells) move less in the sample axis direction as compared to that in the cross section (Fig. 3). In other words, flotation of air cells along the sample axis does not occur, or we did not observe it occurring. This observation suggests that macro-fluid flow was largely inhibited due to the increased viscosity of the unfrozen

matrix due to the stabilizers present in the ice cream samples, which would inhibit the mobility of air cells [14]. In addition, it is also difficult to identify if drainage, which can play an important role in the instability of the air structure at high temperature [14], occurred in this work. However, it is also mentioned that microscopic fluid flow in the channels within the unfrozen matrix probably still occurs which cannot be resolved by the technique used in this work.

3.2 3D Ice crystal evolution

The volume fraction of ice crystals was examined first (Fig. 1), together with the calculated data based on the thermal properties (i.e. extrapolated melting points at various concentrations) of the ice cream formulation. Generally, the results measured by tomography compare well with the theoretical predictions. Minor errors might be caused by shrinkage and expansion, which would change some of the features measured.

Fig. 4 shows the 3D evolution of ice crystals during a thermal cycle. Ice crystals are individually color-rendered according to the equivalent diameter of each ice crystal. In the figure, the blue color corresponds to small size. As expected, ice crystals gradually decreased in size when the sample was heated, reaching the minimum size at -5 ^{o}C. This is consistent with the observation that more small blue ice crystals were present at -5 ^{o}C, as shown in Fig. 4(c). The ice crystals then continuously grew in size when the sample was cooled again to -15 ^{o}C (Fig. 4(d-e)).

Detailed examination of the position change for the 3D ice crystals after heating shows that the ice crystals moved upwards slightly, by less than 20 μm. This movement

of the ice crystals might be caused by compression due to volume shrinkage, which drives the ice crystals to move upwards towards the center of the sample when the unfrozen matrix is less viscous at warmer temperatures [34].

The ice crystals in Fig. 4 were quantified in terms of equivalent diameter and size distribution (Fig. 5). The average equivalent diameter of ice crystals decreases upon heating from 101 μm at -15 ^{o}C to 87 μm at -5 ^{o}C, and then increases again to ~103 μm at -15 ^{o}C after cooling (Fig. 5(a)). Interestingly, the average equivalent diameter of the ice crystals is increased by ~ 2 μm at -15 ^{o}C after a thermal cycle (Fig. 5(a)), suggesting a mild coarsening of ice crystals after thermal cycling. This coarsening of ice crystals at a storage temperature (e.g. -5 ~ -18 ^{o}C) with imposed oscillation temperatures (e.g. ±2.5 ^{o}C) have been previously observed [10, 23, 35, 36]. It is pointed out that the performed thermal cycling in this study leads to much higher coarsening rates than isothermal storage at a certain temperature due to the temperature oscillations which, through observed melting-recrystallization process, increases the rate of the coarsening process [23].

The size distribution of the ice crystals at different temperatures was analyzed and the results are plotted in Fig. 5(b-d). In general, the size distribution curves reflect the temperature change, where the curves shift to the left upon heating (Fig. 5(c)), while they shift to the right during the cooling stage (Fig. 5(d)). It is also shown in Fig. 5(b) that the distribution of the two curves at -15 ^{o}C, before and after the thermal cycle, is similar indicating only a minor change in the overall size after the thermal cycle was completed. This observation confirms that the ice crystals follow mainly a “melting-

recrystallization" mechanism and that other proposed mechanisms [37] play a small or negligible role.

Fig. 6 shows the morphological evolution of five individually separated ice crystals extracted for detailed examination. The morphology of the ice crystals changed during thermal cycling being more irregular at low temperature, e.g. -15 ^{o}C (Fig. 6(a) and (f)), while they became more spherical at "high" temperature, e.g. -5 ^{o}C (Fig. 6(c) and (d)).

The five ice crystals shown in Fig. 6 are quantified in terms of volume, volume change, specific surface area and sphericity, and the results are presented in Fig. 7. It is seen that the volume of each ice crystal keeps decreasing during heating and then increasing during cooling. The volume change (as compared to -15 ^{o}C before thermal cycling) shows that the volume of four of the ice crystals increased by 5.5-11%, indicating an increase in size of ice crystals, which is consistent with the observation of the overall increased equivalent diameter of ice crystals due to coarsening (Fig. 5(a)). However, the volume of ice crystal 3 decreased slightly, by ~4%. This ice crystal is one of the smallest of the 5, and most likely the other four ice crystals grew at the expense of ice crystal 3 via an Ostwald Ripening mechanism [37].

In this study, complete melting of ice crystals was not observed when the sample was heated to -5 ^{o}C since the smallest crystals will have dissolved in the seven thermal cycles prior to the *in situ* experiment. After seven cycles the ice crystals have grown to a large enough size such that they don't completely melt during heating to -5 ^{o}C. This critical size can be extracted from Fig. 5(b). Note that the smallest crystals measured are about 60 μm diameter at -15 ^{o}C, and reduce in size by ~25 μm when heated to -5

^{o}C. This observation suggests that ice crystals with an equivalent diameter less than 25 μm have a high probability of being completely melted during the applied thermal cycling. This is further supported by the observation that there is no significant number of crystals less than 30 μm diameter at -5 ^{o}C. This finding confirms the measurements made in our previous study (i.e. Fig. 9(d) in ref. [5]) showing a significant reduction in the number of ice crystals during the first 7 cycles.

As mentioned, the morphology of ice crystals also changes during thermal cycling (Figs. 3 and 6). This change is quantified using measures of specific surface area and sphericity in Fig. 7 (c) and (d). For example, both the values of specific surface area and sphericity increased continuously as the ice crystals melt, decreasing as the ice crystals recrystallized. These changes support the observation that ice crystals become more spherical during melting (to minimize interfacial energy) and then became more facetted (irregular) during the recrystallization stage as they strive to reach the Wulff shape driven by anisotropy in interfacial energy [38, 39]. However, the ice crystals show only minor morphological changes after a thermal cycle, as indicated by the average sphericity of more than 300 ice crystals where the value increased from ~0.80 at -15 ^{o}C to 0.84 at -5 ^{o}C during the heating stage, and then decreased to ~0.80 when cooled back to -15 ^{o}C. A similar trend was observed for the specific surface area. The minor changes to the size and morphology of ice crystals after one thermal cycle support our previous findings that only small differences in size and morphology of ice crystals were observed between the sample thermally cycled for 7 days and the sample cycled for 14 days [5].

3.3 Unfrozen matrix evolution

Fig. 8 and supplementary Fig. S2 (larger volume) show the 3D morphological evolution of the unfrozen matrix during a thermal cycle. The unfrozen matrix forms a very complex 3D network-like shape with ice crystals and air bubbles dispersed within the matrix. The 3D images in Fig. 8(a-f) show that the unfrozen matrix appeared thicker between air cells upon heating, while they became thinner as the sample cooled down presumably due to the melting of the ice crystals during heating and recrystallization during cooling. This is reflected by the quantified thickness of the unfrozen matrix analyzed in a 721×721×504 μm^3 volume (supplementary Fig. S2), as plotted in Fig. 8(g) where the thickness monotonically increased from ~12.6 μm at -15 ^{o}C to 27.0 μm at -5 ^{o}C, and then decreased to ~19.6 μm at -15 ^{o}C at the end of the thermal cycle.

Figure 8 shows that the thickness of the unfrozen matrix is greater during the cooling stage than during the heating stage, such that the thickness increases by ~ 6 μm after the thermal cycle was completed. After detailed examination, we propose that the formation of a local region of the matrix (e.g. upper right corner in Fig. 3) that is concentrated with more water molecules, is responsible for this change. The shrinkage of the sample, and the associated macro-flow induced by the compression effect, might have accelerated the formation of a larger region of low viscosity matrix. During the cooling stage, no additional new ice crystals were nucleated under the cooling rate studied. Thus, the measured thickness of the unfrozen matrix in this region is higher compared to that before thermal cycling.

In addition, the ‘strength’ (or viscosity) of the unfrozen matrix would decrease at the higher temperatures during heating due to a reduction in viscosity allowing more movement of the matrix to accommodate the overall shrinkage of the sample (see above). Thus, a shift of the structure was observed during the heating stage, suggesting a significant negative impact of the ice melting process on structural stability.

3.4 3D air cell evolution

A few 3D air cells were extracted to examine the coarsening mechanism. Fig. 9 shows one example where two separate air cells gradually merge into one. It is observed that the air cells at -15 ^{o}C are not necessarily round, instead, they have many concave regions (indicated by an arrow in Fig. 9(a)), or even an elongated shape for some cases as seen in Fig. 3. Upon heating, the two air cells merged by creating a bridge between them (Fig. 9(b)), and then the bridge (or neck) continued to thicken with increasing temperature during the heating stage. Meanwhile, some of the concave regions on the air cell surface gradually disappear forming a smooth or spherical surface. The gradual rounding was driven by the reduction in surface energy of the air/unfrozen matrix interface [40].

Decreased viscosity of the unfrozen matrix at “warmer” temperatures upon heating increases the diffusion rate of gas between air cells and promotes coalescence of air cells. It is mentioned that adding stabilizers and emulsifier to ice cream helps reduce air cell coarsening, due to the increased extent of fat destabilization and the increased viscosity of the matrix phase, respectively [14]. It is also noticed that the surrounding

ice crystals significantly affect the shape of the area around the neck between merging cells. One example is shown in Fig. 9(d-2). It is likely that those ice crystals in the vicinity of the neck limit further coalescence of the two air cells due to the constraint imposed by the ice crystal imbedded unfrozen matrix (also see supplementary Fig. S3).

Upon cooling, some of the phenomena observed during the heating stage act in reverse. That is, the surface of air cells became rough or even distorted again at "cooler" temperatures, e.g. -12 ^{o}C in Fig. 9(g). This is most obvious at the lowest temperature of -15 ^{o}C (Fig. 9(h) and (h-2)). The changes are likely to be caused by two main factors. One is that the growing ice crystals continue to push towards the air cells through the unfrozen matrix. This is realized more easily when the unfrozen matrix becomes thinner and thinner as more water molecules are attached to the recrystallizing ice crystals. In total, twenty ice crystals were observed to grow around the air cells shown in Fig. 9 (see supplementary Fig. S3). The second factor is that the pressure within the air cell decreases with the decreasing temperature according to the ideal gas law (PV=nRT), releasing some of the force on the surface that resists morphological change. It is mentioned that the final morphological change is a result of competition between the force imposed on the air cell surface by the growing ice crystals and the surface tension of the air cell/matrix interface. It seems that for the case in Fig. 9 the force imposed by the growing ice crystals through the matrix was greater than the surface tension at temperatures lower than ~ -12 ^{o}C, under which the surface started to deform significantly. In addition, the coalescence process seemed to be inhibited by the increased viscosity at low temperatures during the cooling stage, indicating a

significantly reduced rate of morphological change of the air cells than during the heating stage.

Pelan et al. [41] and Rohenkohl and Kohlus [42] both suggested that the coalescence of air cells to create large coarsened air pockets was the major destabilizing mechanism in the ice cream they studied. A previous study revealed that the storage of ice cream without emulsifier or stabilizer at -15 ^{o}C for 16 days lead to interconnected channels [14]. Our recent observations also showed that thermal cycling of ice cream between -15 and -5 ^{o}C for 14 days resulted in a very complex interconnected air structure [5]. Although Ostwald ripening was observed in the aerated emulsions [43], the *in situ* observations in this study strongly suggest that for ice cream that was cycled for seven times coalescence is the dominant mechanism responsible for the creation of complex interconnected air structures. It should be noted that gas formation can occur due to radiation damage, resulting in molecular bond cleavage (H-H and O-O) or water photolysis, as reported in water under high pressures [44]. If this is occurring, it could explain the increase in bubble volume fraction and the coarsening of bubbles. However, the increase in bubble volume will not have a significant impact on the coarsening of the ice crystals. Gas formation due to irradiation is an open question, as is how this might affect bubble coarsening.

Apart from the coarsening of air cells, another interesting phenomenon was observed, i.e. the reduced volume of some of the air cells after thermal cycling. Fig. 10 shows the evolution of three individually extracted air cells during thermal cycling, and their corresponding quantified volume changes are plotted in Fig. 11. The overall

volume fraction of air cells was also analyzed and the result was observed to decrease monotonically during the heating stage, and continued to decrease until 0.256 at ~ -7 ^{o}C during cooling before it started to rise upon further freezing (Fig. 11(a)). The volume fraction after the thermal cycle (~ 0.285) was lower compared to that before thermal cycling began (~0.330). This corresponds to a reduction of volume fraction by ~ 13.8%. The trend of the volume change of the three individual air cells is consistent with that for the overall volume change. It is also noticed that the change of volume is even more than 50% for Air 2 and Air 3, and that those two air cells did not grow in size during the cooling stage. Detailed mechanisms here are still unknown. It is unlikely that the hydrostatic pressure causes such a large change, as the sample height is quite small. The shift of the sample during the thermal cycle might contribute to some measurement errors; however, we believe the volume (thus size) change of the air cells is the main contribution, which is supported by the volume change of all three air cell cases (Fig. 11(c-d)). We suspect that the diffusion of gas into the matrix and the surrounding air cells, as well as out of the whole sample, at the warm temperatures might have contributed to this change. The detailed mechanisms will be investigated in our future study.

3.5 Summary of microstructural evolution mechanisms

Here, we summarize the mechanisms that control the microstructural evolution of ice cream as observed in this *in situ* study (Table 1). Generally, the microstructural evolution of ice cream during thermal cycling is controlled by the interaction of three phases.

Regarding ice crystals, nucleation of new ice crystals does not occur under the cooling condition studied in this work. The melting-recrystallization mechanism hypothesized as an important mechanism in our previous study [5] was quantified by analyzing the 4-D tomographs during the thermal cycle. The melting and recrystallization of ice crystals also affects the air cell's morphology, as well as its coarsening process, through the unfrozen matrix layer between the ice crystals and the air structures. For the air phase, coalescence of air cells is clearly observed to be responsible for the coarsening mechanism. For the sample that was initially thermally cycled for seven times, Ostwald ripening takes a less important role in the coarsening of both ice crystals and air cells during thermal cycling. The continuous reduction of air cell volume needs further investigation. The third phase, the unfrozen matrix, is a crucial component controlling the microstructural stability of ice cream. It acts as the reservoir for the water from dissolving ice during heating and releases water for recrystallization of the ice crystals during the cooling cycle. The network of unfrozen matrix, reinforced by the distributed ice crystals (and dissolved hydrocolloids), holds the whole structure together and greatly influences the structural stability of ice cream when subjected to external temperature variations.

4. Conclusions

Using 4D synchrotron X-ray tomography, we investigated the effect of thermal variation on the microstructural stability of ice cream during a heating and cooling cycle between -15 ^{o}C and -5 ^{o}C, at a ramp rate of 0.05 ^{o}C/min. A new data reconstruction and

image processing method was developed, enabling the large 4D data sets to be segmented and quantified. The experimental set-up, as well as the image processing routine developed, can be applied to a wide range of soft materials.

The dynamic evolution of individual microstructural features, i.e. an ice crystal, air cell, and unfrozen matrix, was quantitatively analyzed. The findings integrate the *ex situ* observations made in our previous work enhancing our understanding of the mechanisms controlling ice cream's microstructural evolution. The experimental results in this study reveal important physical mechanisms that influence microstructural instability: that is, the coarsening of air cells takes place mainly through the coalescence of neighboring air cells, while ice crystal growth results from the melting-recrystallization mechanism during thermal cycling, both of which lead to degradation of ice cream's microstructure. The unfrozen matrix plays an important role in maintaining the integrity of the structure of ice cream while being flexible enough at the higher temperatures to reduce the stresses imposed during heating and then cooling by the melting and recrystallization of the ice crystals.

Acknowledgements

This work was financially supported by Unilever R&D (Colworth, U. K) and in part by the EPSRC (EP/I02249X/1, EP/J010456/1 and EP/M009688/1). The authors acknowledge the use of the facility access in Diamond Light Source (MT12194, MT12195 & MT12616) and Research Complex at Harwell. The authors also thank I13 staff of Diamond Light Source (especially Drs. Rau, Wanelik, Cipiccia and Marathe) and group members for technical support.

Data statement

Representative samples of the research data are shown in the figures. Other datasets generated during and/or analysed during this study are not publicly available due to their large size but are available from the corresponding author on reasonable request.

References

[1] R.G.M. van der Sman, A.J. van der Goot, The science of food structuring, Soft Matter 5(3) (2009) 501-510.

[2] J. Ubbink, A. Burbidge, R. Mezzenga, Food structure and functionality: a soft matter perspective, Soft Matter 4(8) (2008) 1569-1581.

[3] A. Kovalenko, K. Zimny, B. Mascaro, T. Brunet, O. Mondain-Monval, Tailoring of the porous structure of soft emulsion-templated polymer materials, Soft Matter 12(23) (2016) 5154-5163.

[4] B. R. Pinzer, A. Medeback, H. J. Limbach, C. Dubois, M. Stampanoni and M. Schneebeli, 3D-characterization of three-phase systems using X-ray tomography: tracking the microstructural evolution in ice cream, Soft Matter, 2012, 8, 4584 (8) (2012) 4584-4594.

[5] E.Y. Guo, G. Zeng, D. Kazantsev, P. Rockett, J. Bent, M. Kirkland, G. Van Dalen, D.S. Eastwood, D. StJohn, P.D. Lee, Synchrotron X-ray tomographic quantification of microstructural evolution in ice cream - a multiphase soft solid, RSC Advances 7(25) (2017) 15561-15573.

[6] G.V. Dalen, A study of bubbles in foods by X-ray microtomography and image analysis, Microscopy and Analysis 26(2) (2012) S8-S12.

[7] C. Clarke, The Science of Ice Cream, CPI Group (UK) Ltd, Croydon, UK , 2012.

[8] H. Matthias D. Eisner, E.J.Windhb, Air cell microstructuring in a high viscous ice cream matrix, Colloids and Surfaces A: Physicochem. Eng. Aspects 263 (2005) 390-399.

[9] A.P. Paula Varela, S. Fiszman, How hydrocolloids affect the temporal oral perception of ice cream, Food Hydrocolloids 36 (2014) 220-228.

[10] M. Tsevdou, E. Gogou, E. Dermesonluoglu, P. Taoukis, Modelling the effect of storage temperature on the viscoelastic properties and quality of ice cream, Journal of Food Engineering 148 (2015) 35-42.

[11] J.J. Cheng, J. Cui, Y. Ma, T.S. Yan, L.F. Wang, H. Li, X.S. Li, Effects of soy-to-milk protein ratio and sucrose fatty acid ester addition on the stability of ice cream emulsions, Food Hydrocolloids 60 (2016) 425-436.

[12] J.V. Patmore, H.D. Goff, S. Fernandes, Cryo-gelation of galactomannans in ice cream model systems, Food Hydrocolloids 17(2) (2003) 161-169.

[13] A. Regand, H.D. Goff, Structure and ice recrystallization in frozen stabilized ice cream model systems, Food Hydrocolloids 17 (2003) 95-102.

[14] Y. Chang, R.W. Hartel, Stability of air cells in ice cream during hardening and storage, Journal of Food Engineering 55 (2002) 59-70.

[15] K.L.K. Cook, R.W.Hartel, Effect of freezing temperature and warming rate on dendrite break-up when freezing ice cream mix, International Dairy Journal 21 (2011) 447-453.

[16] Y. Chang, R.W. Hartel, Development of air cells in a batch ice cream freezer, Journal of Food Engineering 55 (2002) 71-78.

[17] A. Caillet, C. Cogne, J. Andrieu, P. Laurent, A. Rivoire, Characterization of ice cream structure by direct optical microscopy. Influence of freezing parameters, Lebensmittel-Wissenschaft Und-Technologie-Food Science and Technology 36(8) (2003) 743-749.

[18] J.J. Cheng, Y. Ma, X.S. Li, T.S. Yan, J. Cui, Effects of milk protein-polysaccharide interactions on the stability of ice cream mix model systems, Food Hydrocolloids 45 (2015) 327-336.

[19] E. Faydi, J. Andrieu, P. Laurent, Experimental study and modelling of the ice crystal morphology of model standard ice cream. Part I: Direct characterization method and experimental data, Journal of Food Engineering 48 (2001) 283-291.

[20] K.B. Caldwell, H.D. Goff, D.W. Stanley, R.W. Martin, A low-temperature scanning electron microscopy study of ice cream. 1. Techniques and general microstructrure, Food Structure 11(1) (1992) 1-9.

[21] A.A. Flores, H.D. Goff, Ice crystal size distributions in dynamically frozen model solutions and ice cream as affected by stabilizers, Journal of Dairy Science 82(7) (1999) 1399-1407.

[22] C. Mendez-Velasco, H.D. Goff, Fat structure in ice cream: A study on the types of fat interactions, Food Hydrocolloids 29(1) (2012) 152-159.

[23] G.A. Fatou Toutie Ndoye, Characterization of ice recrystallization in ice cream during storage using the Focused Beam Reflectance Measurement, Journal of Food Engineering 148 (2015) 24-34.

[24] E.Y. Guo, A.B. Phillion, B. Cai, S.S. Shuai, D. Kazantsev, T. Jing, P.D. Lee, Dendritic evolution during coarsening of Mg-Zn alloys via 4D synchrotron tomography, Acta Materialia 123 (2017) 373-382.

[25] K.M. Kareh, P.D. Lee, R.C. Atwood, T. Connolley, C.M. Gourlay, Revealing the micromechanisms behind semi-solid metal deformation with time-resolved X-ray tomography, Nature Communications 5 (2014).

[26] S. Karagadde, P.D. Lee, B. Cai, J.L. Fife, M.A. Azeem, K.M. Kareh, C. Puncreobutr, D. Tsivoulas, T. Connolley, R.C. Atwood, Transgranular liquation cracking of grains in the semi-solid state, Nature Communications 6 (2015).

[27] P. Rockett, S. Karagadde, E. Guo, J. Bent, J. Hazekamp, M. Kingsley, J. Vila-Comamala, P.D. Lee, Iop, A 4-D dataset for validation of crystal growth in a complex three-phase material, ice cream, Mcwasp Xiv: International Conference on Modelling of Casting, Welding and Advanced Solidification Processes2015.

[28] A.C. Kak, M. Slaney, Principles of computerized tomographic imaging, IEEE Press, New York, 2001.

[29] D. Kazantsev, F. Bleichrodt, T. Van Leeuwen, A. Kaestner, P. Withers, K.J. Batenburg, P.D. Lee, A novel tomographic reconstruction method based on the robust Student's t function for suppressing data outliers, IEEE Transactions on Computational Imaging 99 (2017) 1-1.

[30] D. Kazantsev, E.Y. Guo, A.B. Phillion, P.J. Withers, P.D. Lee, Model-based iterative reconstruction using higher-order regularization of dynamic synchrotron data, Measurement Science and Technology 28(9) (2017).

[31] P. Paleo, A. Mirone, Ring artifacts correction in compressed sensing tomographic reconstruction, Journal of Synchrotron Radiation 22 (2015) 1268-1278.

[32] J. Weickert, Anisotropic diffusion in image processing, Stuttgart: Teubner, 1998.

[33] M. Doube, M.M. Klosowski, I. Arganda-Carreras, F.P. Cordelieres, R.P. Dougherty, J.S. Jackson, B. Schmid, J.R. Hutchinson, S.J. Shefelbine, BoneJ Free and extensible bone image analysis in ImageJ, Bone 47(6) (2010) 1076-1079.

[34] H.D. Goff, R.W. Hartel, Ice cream, 7th Edition ed., Springer Science & Business Media, New York,

2013.
[35] D.P. Donhowe, R.W. Hartel, Recrystallization of ice in ice cream during controlled accelerated storage, International Dairy Journal 6(11-12) (1996) 1191-1208.
[36] D.P. Donhowe, R.W. Hartel, Recrystallization of ice during bulk storage of ice cream, International Dairy Journal 6(11-12) (1996) 1209-1221.
[37] K.L.K. Cook, R.W. Hartel, Mechanisms of Ice Crystallization in Ice Cream Production, Comprehensive Reviews in Food Science and Food Safety 9(2) (2010) 213-222.
[38] G. Wulff, On the question of speed of growth and dissolution of crystal surfaces, Zeitschrift Fur Krystallographie Und Mineralogie 34(5/6) (1901) 449-530.
[39] R. Shuttleworth, The surface tension of solids, Proceedings of the Physical Society of London Section A 63(365) (1950) 444-457.
[40] P. Walstra, Dispersed systems: basic consideration, in: O.R. Fennema (Ed.) Marcel Dekker., New York, 1996, pp. 95-115.
[41] B.M.C. Pelan, K.M. Watts, I.J. Campbell, A. Lips, The stability of aerated milk protein emulsions in the presence of small molecule surfactants, Journal of Dairy Science 80(10) (1997) 2631-2638.
[42] H. Rohenkohl, R. Kohlus, Foaming of ice cream and the time stability of its bubble size distribution, in: G.M. Campbell, C. Webb, S. Pandiello, K. Niranjan (Eds.) Bubbles in food, MN: Eagan Press., 1999, pp. 45-53.
[43] G.V. Dalen, M.W. Koster, μCT imaging of aerated emulsions, SkyScan user meeting, Leuven, Belgium, 2011.
[44] W.L. Mao, H.K. Mao, Y. Meng, P.J. Eng, M.Y. Hu, P. Chow, Y.Q. Cai, J.F. Shu, R.J. Hemley, X-ray-induced dissociation of H2O and formation of an O-2-H-2 alloy at high pressure, Science 314(5799) (2006) 636-638.

Figures

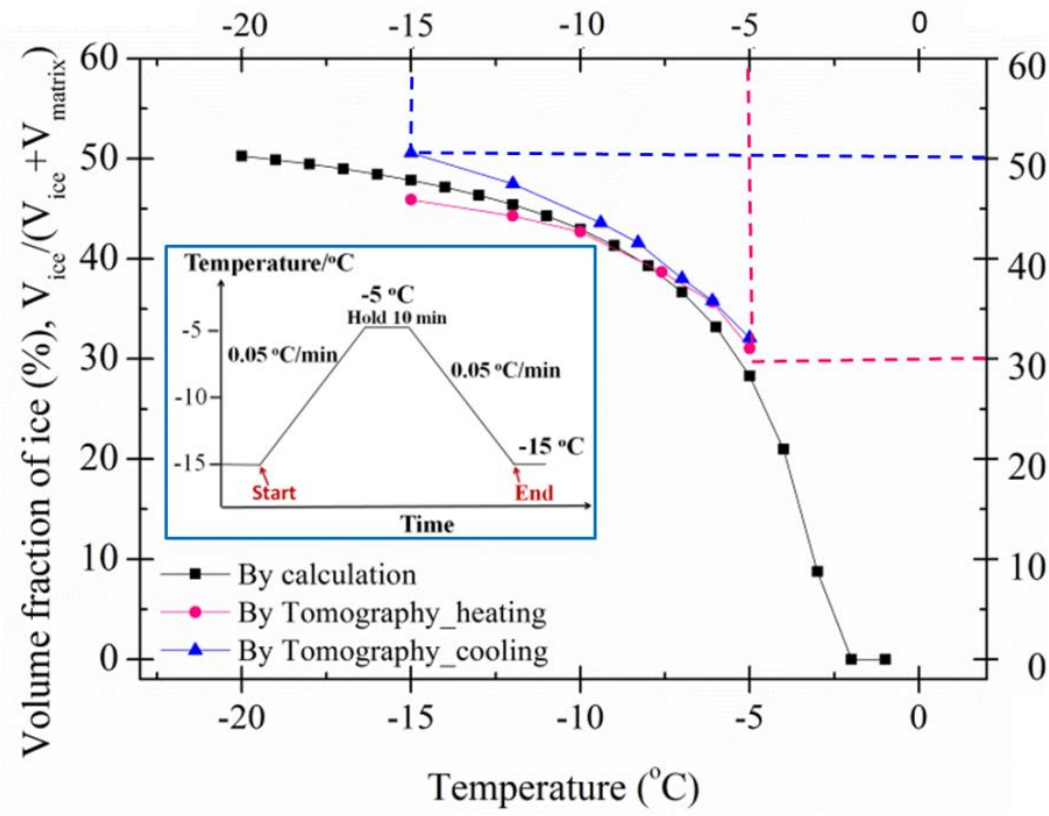

Fig. 1 Change in ice volume fraction as a function of temperature. The inset shows the thermal cycling history of the ice cream sample for the *in situ* synchrotron experiment. The measured phase diagram (i.e. extrapolated melting points at various concentrations) of the ice cream formulation is presented in [5].

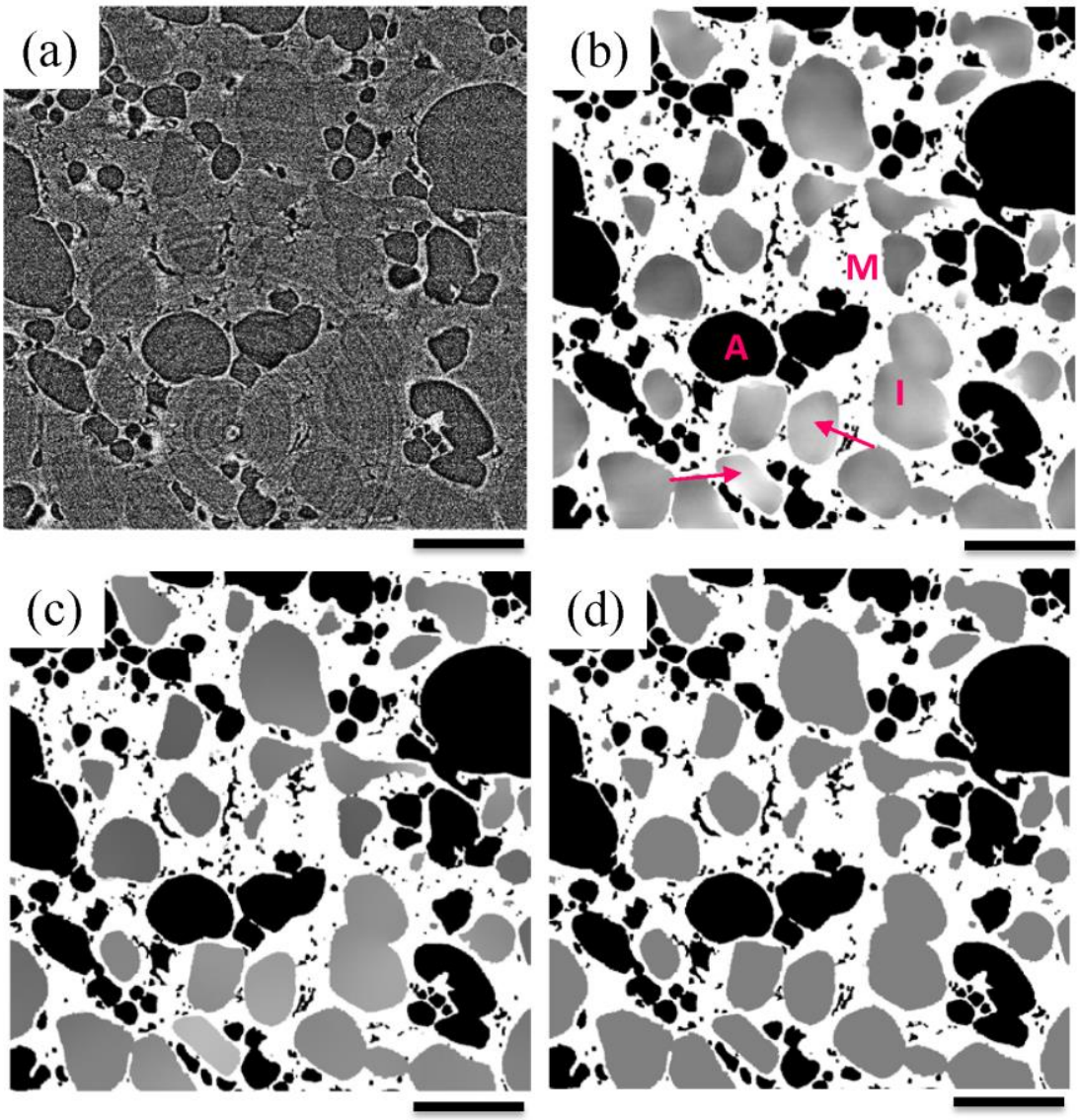

Fig. 2 Reconstructed images using (a) conventional FBP reconstruction method and (b) MBIR reconstruction method; (c) post-processed image of reconstructed MBIR image of (b), note more homogeneous (equalized) intensities compared to (b) within ice-crystals; (d) 3-phases segmentation using (c). A, I and M in (b) stand for air cell, ice crystal and unfrozen matrix, respectively. Scale bar =150 μm.

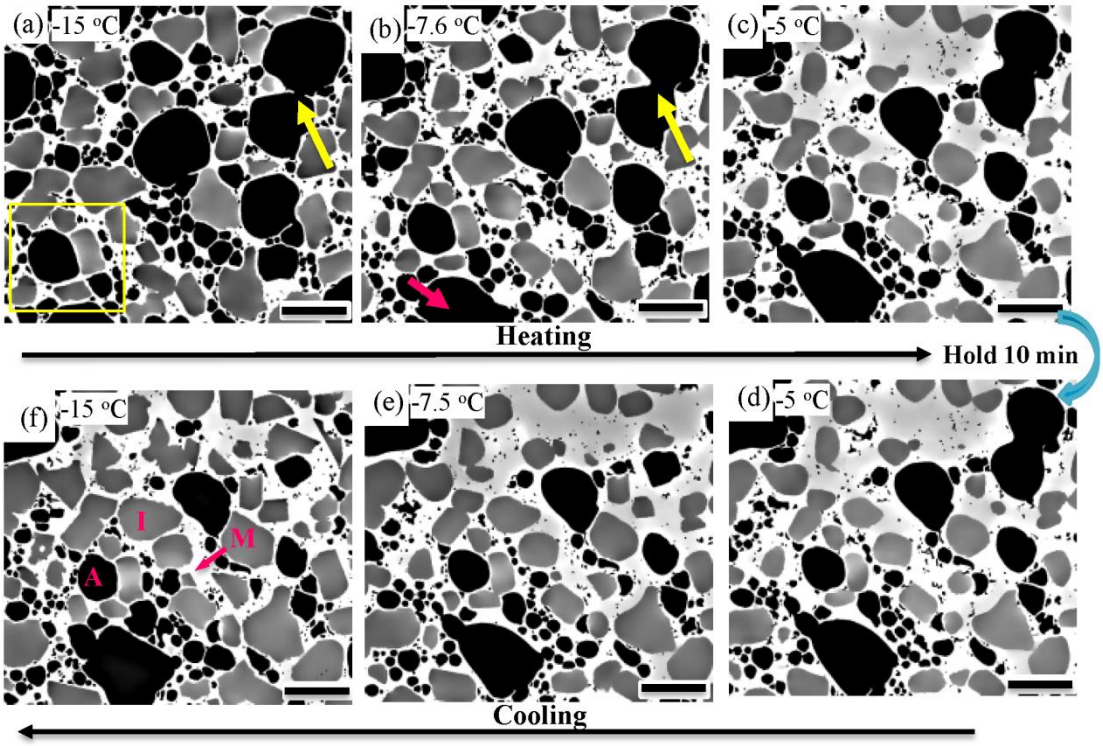

Fig. 3 Reconstructed tomographic slices (prior to the equalization step) showing the overall microstructural evolution of ice cream during a thermal cycle: (a) -15 °C, (b) -7.6 °C, and (c) -5 °C during heating, (d) after holding at -5 °C for 10 min, (e) -7.5 °C, and (f) -15 °C during refreezing. A, I and M in (f) stand for air cell, ice crystal and unfrozen matrix, respectively. Scale bar equals 150 μm.

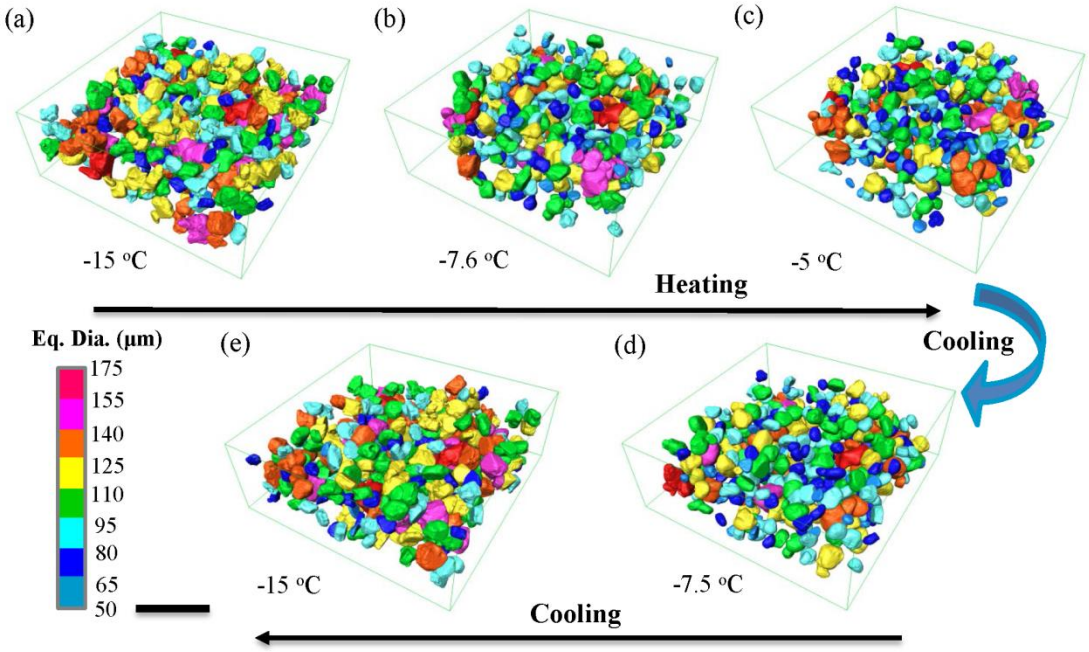

Fig. 4 3D ice crystal evolution in a 1416×1416×504 μm^3 volume during a thermal cycle: (a) -15 °C, (b) -7.6 °C, (c)-5 °C, (d) -7.5 °C, and (e) -15 °C. Ice crystals are size-colored using the equivalent diameter. Scale bar equals 500 μm.

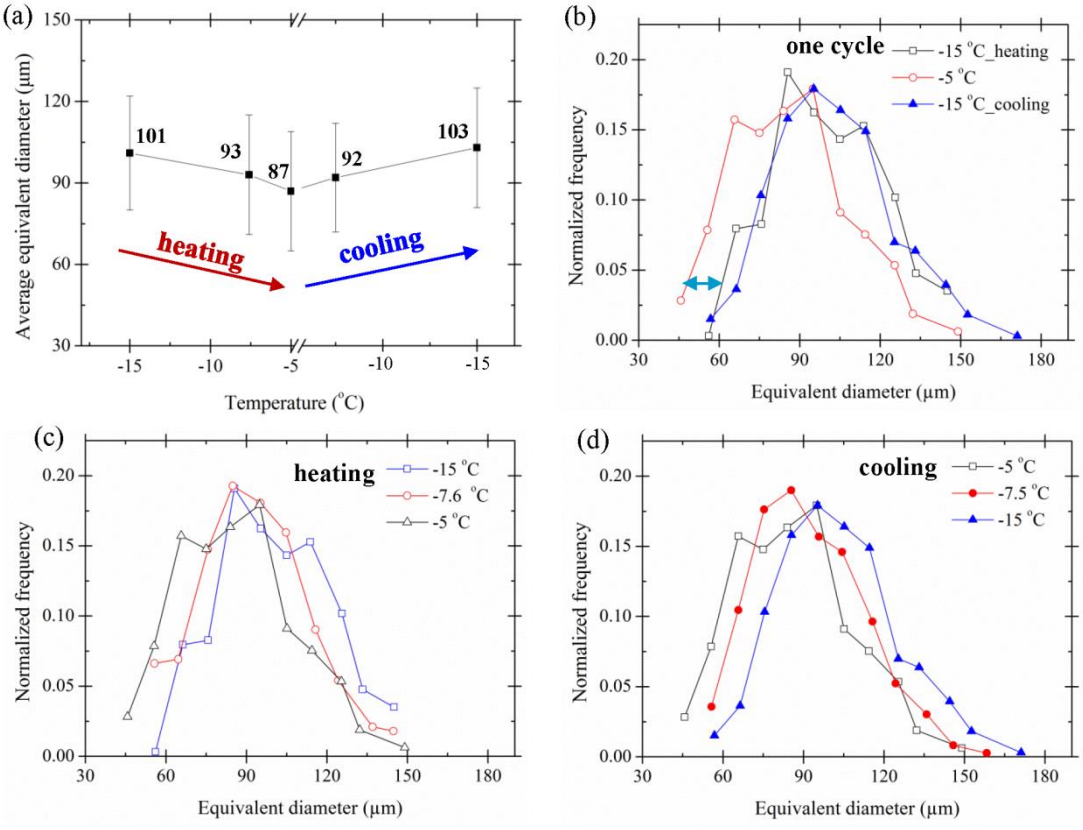

Fig. 5 Quantified ice crystal size during a thermal cycle: (a) change of average equivalent diameter of ice crystals during a thermal cycle; (b-d) size distribution of ice crystals during (b) a complete thermal cycle, (c) heating stage and (d) cooling stage. The arrow in (b) indicates the size shift of the curves. Note, more than 300 ice crystals were analyzed.

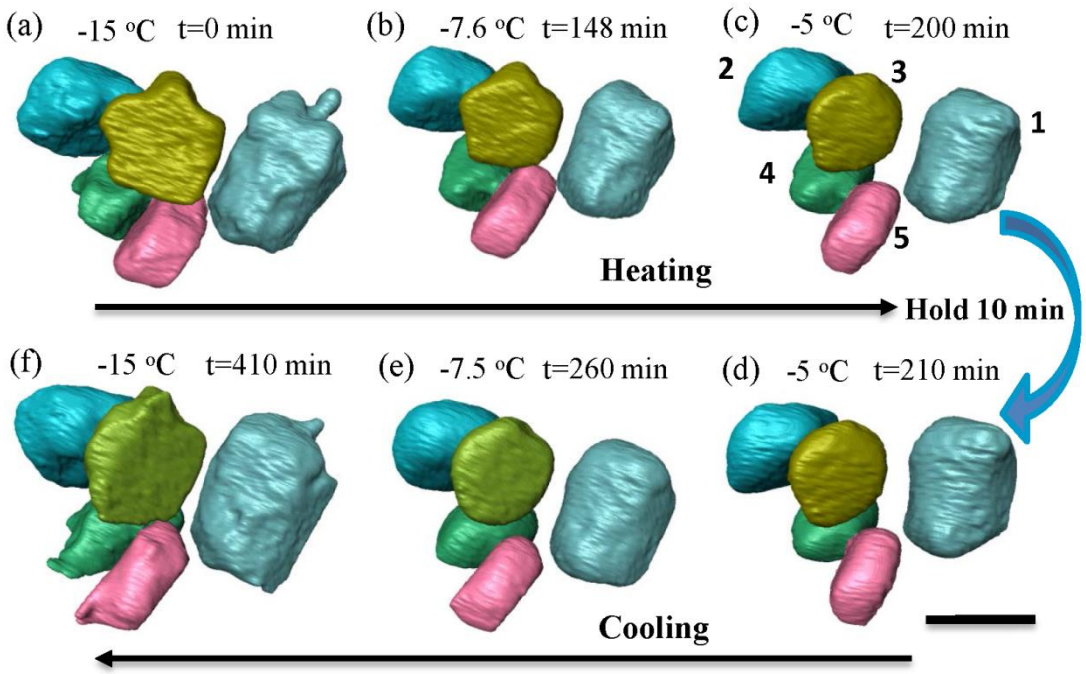

Fig. 6 3D morphological evolution of five ice crystals during a thermal cycle: (a) -15 °C, (b) -7.6 °C, (c) -5 °C, (d) after holding at -5 °C for 10 min, (e) -7.5 °C, and (f) -15 °C. The time is indicated in each figure during the thermal cycle. Scale bar 150 μm for all images. Numbers in (c) match the ice crystals analyzed in Fig. 7.

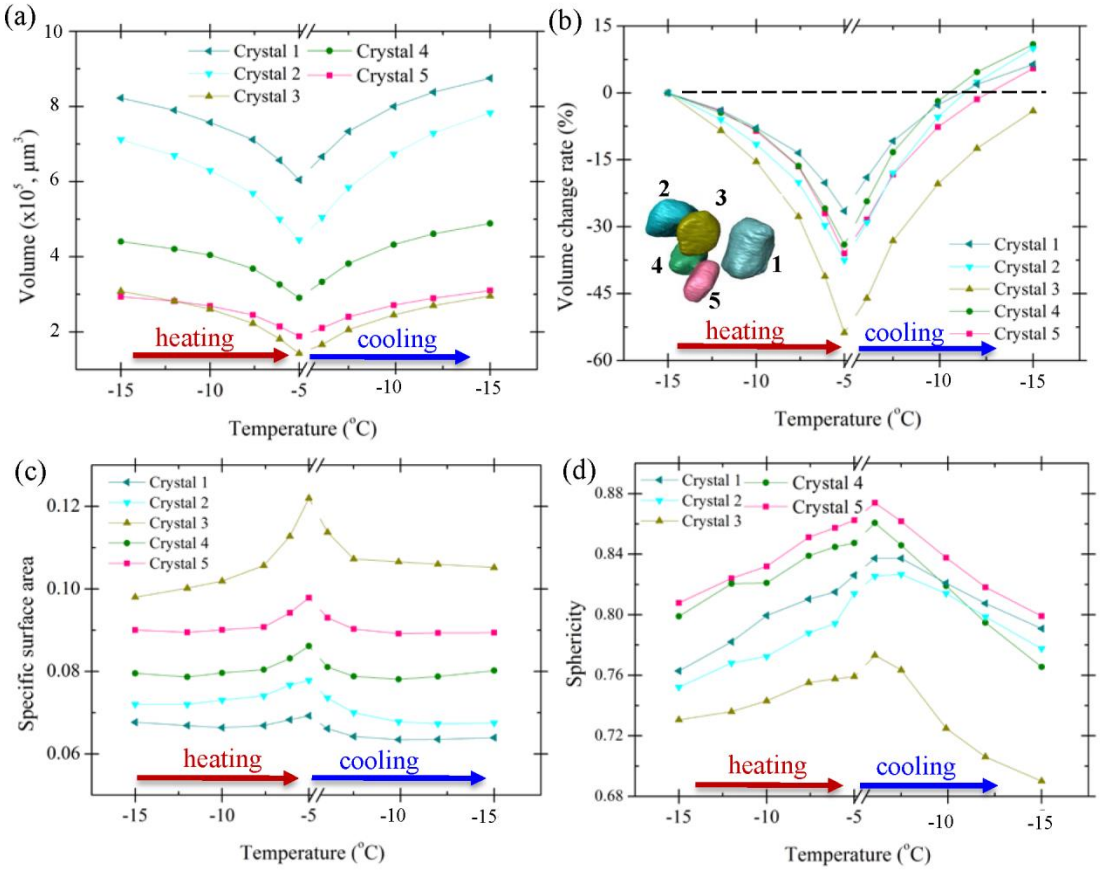

Fig. 7 Quantified results of five ice crystals during a thermal cycle: (a) volume, (b) volume change, (c) specific surface area, and (d) sphericity. Note the colours of the plots in each figure are identical to the colour-rendered ice crystals in (b).

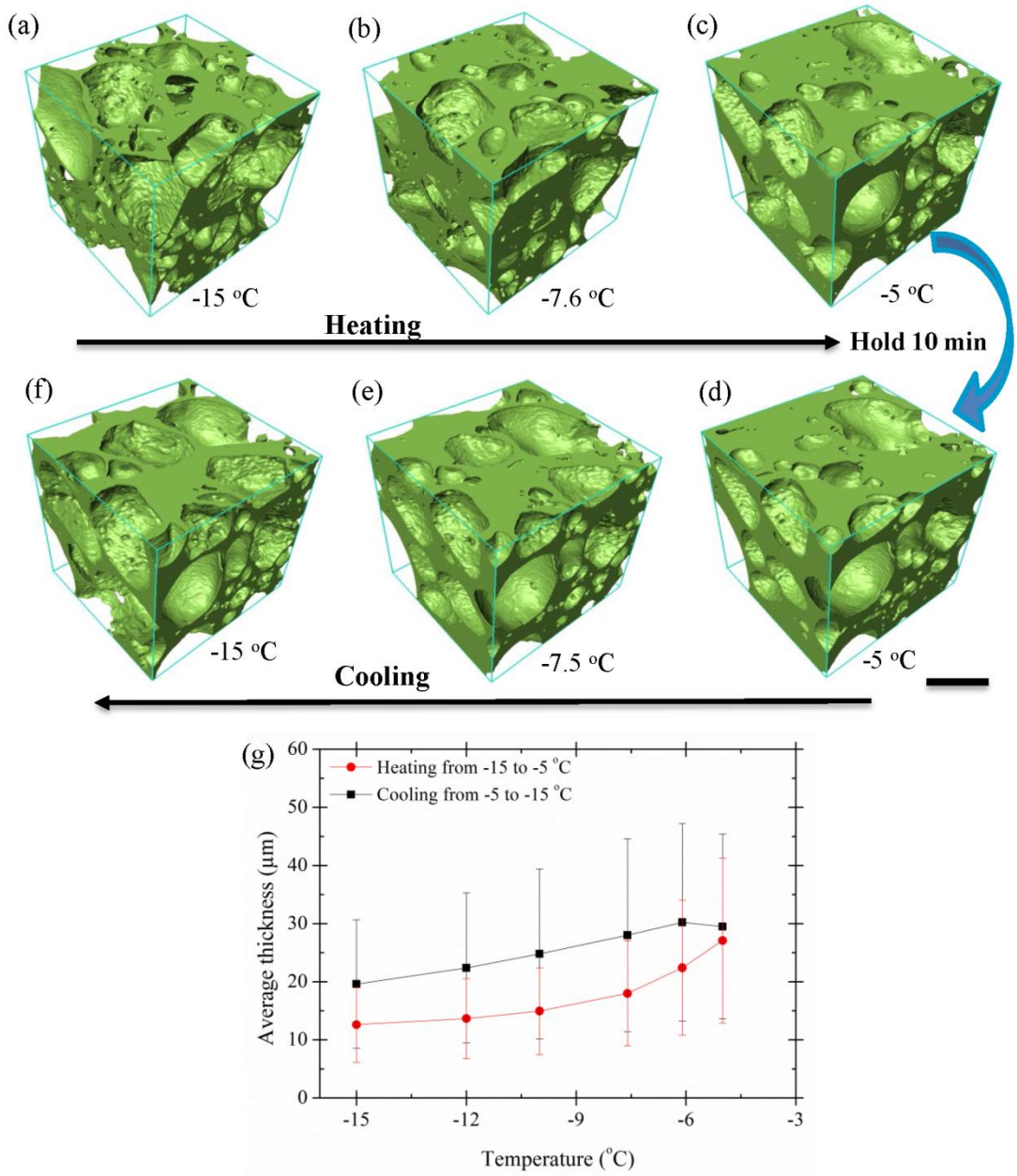

Fig. 8 3D morphological evolution of unfrozen matrix within a 259×243×243 μm^3 volume during a thermal cycle: (a) -15 °C, (b) -7.6 °C, (c) -5 °C, (d) after holding at -5 °C for 10 min, (e) -7.5 °C, and (f) -15 °C; (g) Average thickness of the unfrozen matrix as a function of temperature. Note, the thickness is measured within a 721×721×504 μm^3 volume, identical to the domain as shown in supplementary Fig. S2. Figures (a-f) share the same scale bar. Scale bar equals 100 μm.

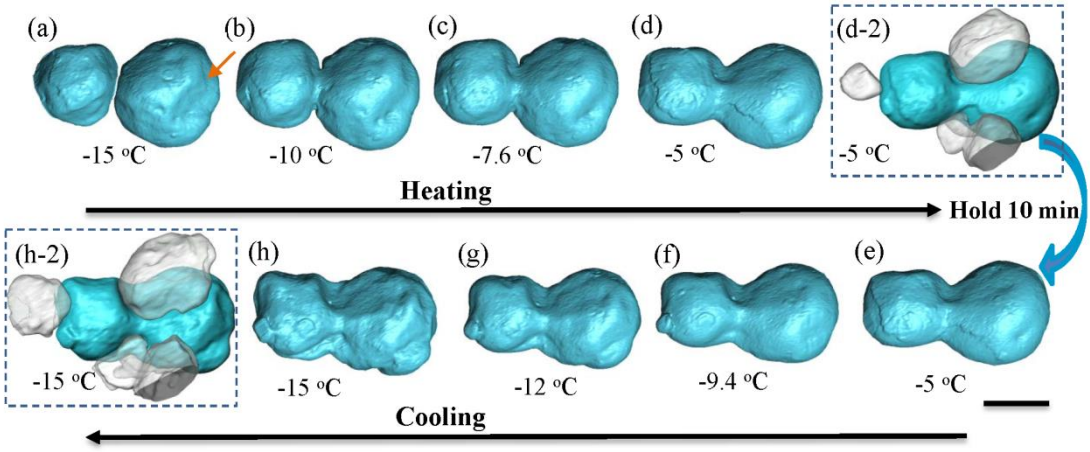

Fig. 9 Coalescence of two air cells during the heating stage (a-d) and cooling stage (e-h) of a thermal cycle. (d-2) and (h-2) show the morphological relationship between the surrounding ice crystals and the air cell at -5 °C and -15 °C, respectively. Scale bar 100 μm for all images.

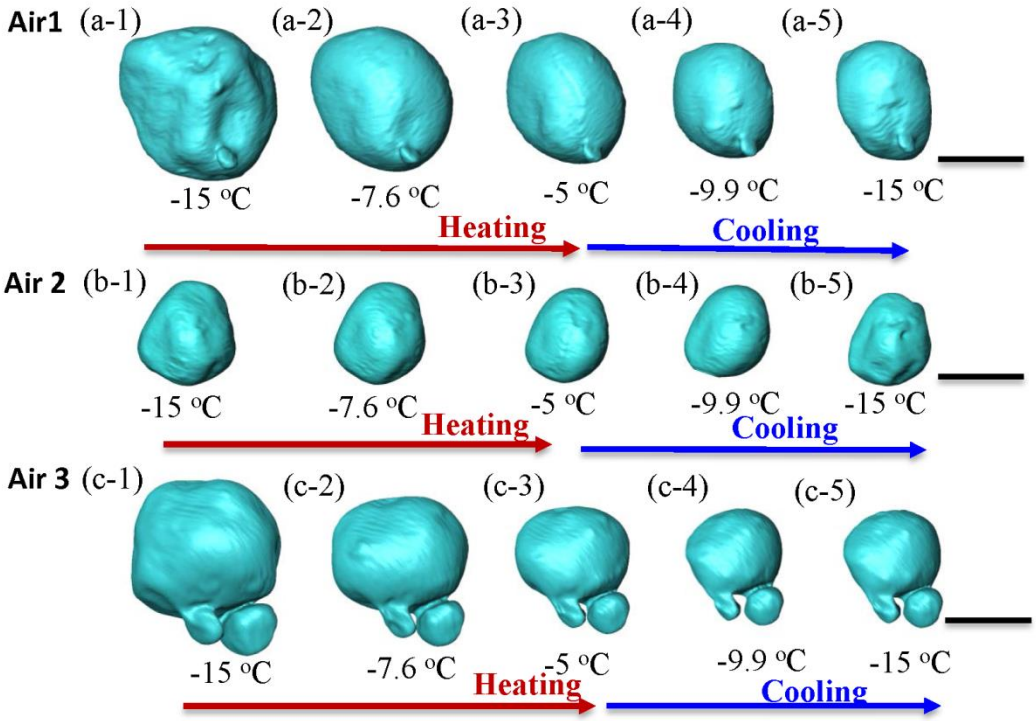

Fig. 10 Morphological evolution of three individual air cell cases during a thermal cycle. Scale bar 100 μm for all images.

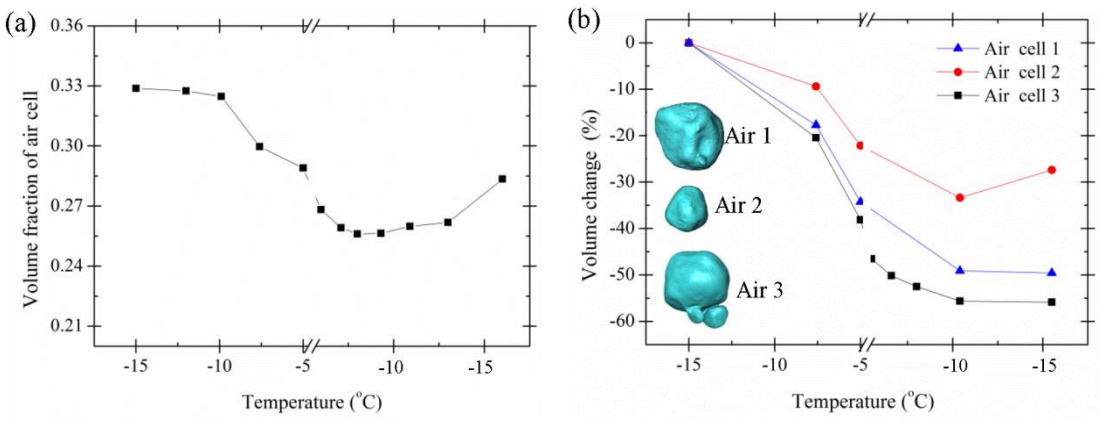

Fig. 11 Volume change of air cells as a function of temperature during a thermal cycle: (a) overall volume change of air cells in a 1416×1416×504 μm^3 volume, (b) volume change of three individual air cells.

Table

Table 1 A summary of the microstructural changes that occur during a thermal cycling from -5 to -15 ºC highlighting the differences between what occurs during the first seven cycles and the following seven cycles. The arrows indicate that part of the cycle over which most change occurs.

	Heat to -5 ºC	**Hold at -5 ºC**	**Cool to -15 ºC**	**Hold at -15 ºC**
		Air cells		
Coalescence of neighbouring air cells.	→			
1 to 7 cycles	Size increases although some small air cells remain leading to a bimodal distribution and remain equiaxed.		The air cells shrink.	Cells remain relatively spherical.
8 to 14 cycles	Coalescence of neighbouring air cells.		The air cells become irregular due to constraint by matrix and ice crystals.	Air cells become interconnected and form channels within the matrix network.
Air cells continue to grow into a large interconnected network of irregular shapes as the number of thermal cycles increase. The morphology is constrained by the network of unfrozen matrix and ice crystals.				
		Ice crystals		
	Melt by ~40%		Grow by ~66%	
	Dissolution		Recrystallization	
	→			
1 to 7 cycles	Size of ice crystals decrease and those < 25 µm melt completely. The morphology becomes rounded.	The size and morphology of crystals change little.	Size of ice crystals increase and no nucleation of new crystals occurs. The morphology becomes irregular during recrystallization.	Over the cycle, the size increases significantly and the number decrease significantly.
8 to 14 cycles	Size decreases by ~ 25 µm dissolvingand the number changes little.	The size of crystals change little.	Size of ice crystals increase by about 25 µm. The number remains unchanged.	Over the cycle, the size increases by a small amount and the number do not increase.
After 7 thermal cycles, the number changes little and the size of ice crystals increase slowly. The ice crystals form networks within the unfrozen matrix network.				
		Unfrozen matrix		
Water content	Increases	High	Decreases	Low
Viscosity	Viscosity decreases	Low	Viscosity increases	High
Mechanical response	Matrix becomes and remains flexible, reducing residual stresses		Matrix becomes less flexible	Matrix is effectively rigid
Total volume	Ice cream expands	May shrink somewhat	Ice cream shrinks	Relatively constant
Alignment of ice crystals with the unfrozen matrix network occurs to minimise surface energy and reduce local stress with each additional thermal cycle. At the warmer temperatures the matrix				

becomes flexible also reducing stresses developed by the constraint of ice crystal and air cells.